Multi-pulse RGB illumination and detection for particle tracking velocimetry

J. Menser[*,1], T. Dreier[1,2], S. Kaiser[1], C. Schulz[1,2]

[1]IVG, Institute for Combustion and Gas Dynamics – Reactive Fluids, University of Duisburg-Essen, Germany
[2]CENIDE, Center for Nanointegration Duisburg-Essen, Duisburg, Germany

Abstract

This work demonstrates the application of low-cost color light sources (LEDs or laser diodes) and detectors with RGB Bayer filter and for particle tracking velocimetry. Glass (55 µm) and polyamide (10 µm) particles were used as tracers in water flows while droplets formed in a nozzle flow were the targets in spray experiments. LEDs were assembled in a side-illumination and shadowgraphic configuration illuminating a larger volume, while the light of the laser diodes was formed into a light sheet. The optical system was characterized and image processing is described.

Introduction

Particle tracking velocimetry (PTV) is commonly used to determine the velocity of immersed particles assumed to follow gaseous and liquid flows. In this technique, subsequent laser pulses separated in time by a variable delay depending on the flow speed volumetrically illuminate a particle-seeded flow. A multi-frame camera detects elastically scattered light. In most such experiments, the illumination and detection devices (laser and scientific camera, respectively) are expensive and sensitive to harsh environments. In the present work, this equipment is replaced by fairly cheap consumer electronics, in particular red/green/blue light-emitting diodes [2-3] (RGB LEDs) or laser diodes and a digital single-lens reflex camera (DSLR) (about 5000 € for the light source, detector and triggering unit). To obtain the time information within a single picture, the red, green, and blue LEDs are pulsed one after the other with a defined delay and pulse length. The RGB sensor of the DSLR detects the scattered light from all three pulses through a sufficiently long exposure time. By separating each image color in post processing, the three time step images can be recovered.

Experimental apparatus

The feasibility of the system was tested in water seeded with particles (either LaVision Vestosint 55 µm 0.5 g/l, or LaVision glass hollow spheres 10 µm 0.1 g/l), and the suspension was stirred by a magnetic mixer. In this arrangement, the mean flow velocity varies between zero and 1 m/s.

Additionally, the movement of gas-borne ethanol droplets was observed that were generated by a 0.4 mm diameter spray nozzle in a coflow of 5 slm O_2, generating flow velocities up to 40 m/s with a sparse droplet distribution [4]. The same device was utilized as a spray flame to visualize unburned spray droplets in a reactive environment. Using LEDs the experiments were done in shadowgraphic and side-illumination (scattering) configuration.

Fig. 1 illustrates the experiment. For detection, a digital single-lens reflex camera (DSLR, Nikon D5100) equipped with a macro lens (f = 105 mm, f/2.8) and bellows was used. The macro lens is set to the closest possible focal position. By shifting the lens with the macro bellows the magnification can be adjusted from 1:1 (highest magnification of the single macro lens) to 3:1 (largest bellows extension). The camera detector has a pixel size of 7.4×7.4 µm^2. To obtain a sizeable image of a 10 µm particle on the detector the magnification must be high enough; otherwise the particle is represented by an Airy disk. Due to lens aberrations and the size of the measurement volume, a magnification of 2:1 was selected. The camera was operated in manual mode for full control of exposure time, aperture size and gain.

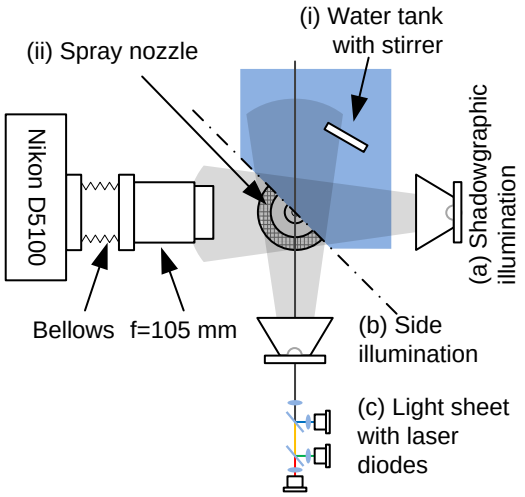

Fig. 1: Illumination and detection geometry of the particle-seeded water tank. The red/green/blue LEDs can be assembled either in 180° (a) or 90° (b) position relative to the detector. Also, laser diodes (c) can be used. Measurements were done in a water tank (i). For further diagnostics a nanoparticle-synthesis spray-flame nozzle (ii) was used.

The size of the water tank is 20×30×40 cm^3. The magnetic stirrer is placed in the center. By changing the rotational speed of magnetic stir bar or by moving the measurement volume the mean speed and vorticity of the particles can be varied.

* Corresponding author: jan.menser@uni-due.de

The LEDs were assembled in a 180° (shadowgraphy) and a 90° (side-illumination) geometry relative to the detector. A parabolic reflector collimated the light to a parallel beam of about 6 cm diameter at the measurement position. The diverging beam of the laser diodes was collimated with f = 4 mm quartz lenses. The resulting beam had a full width (FWHM) of 1 mm. Afterwards the three colors were superposed with a 500 nm, 45° long-pass filter and a 590 nm, 45° short-pass filter. A cylindrical lens (f = 10 mm) expanded the light sheet (1 mm thickness) to a 1 cm height in the probe volume.

Image acquisition

The main objectives of this work are the development of an efficient illumination and detection system together with a proper image post processing.

Calibrating the experimental equipment:

1. Measure the spectral overlap between the light sources and the RGB-filter transmission of the camera sensor.
2. Determine the shortest achievable pulse length and the highest thermal load on electronics when pulsing the LEDs.
3. Estimate the delay time between LED pulses and maximum pulse length considering local flow velocities.
4. Set up camera parameters (gain, aperture size, exposure time).

Measurement workflow:

1. Image acquisition.
2. Image conversion to 16-bit TIFF format.
3. Deconvolution of color cross-talk.
4. Background correction.
5. Import to PTVLab.

Short pulsing of diodes

The pulse length and pulse delay was adjusted with a digital delay generator (Stanford Research Systems, DG645). To switch the electrical current, MOSFET gate drivers were used. The maximum supply voltage is 18 V and the maximum current is 5 A. Due to a varying forward voltage depending on diode temperature and employed as damping of the resonant circuit a series resistor was embedded. However, the resistor limits the rise time of the generated electrical pulses. With common resistors a minimum rise and fall time of 600 ns can be achieved. Low inductance resistors improve this value to about 200 ns. Here, the circuit limits the pulse length to a minimum of about 1 µs.

The maximum power used to operate LEDs is limited by the mean heat release. The applied LEDs have a maximum electrical rating of 1 W. For instance a green LED operated in continuous wave mode requires a forward voltage of 3.4 V and a current of 300 mA. In pulsed mode the voltage is set to 15 V and the current is 5 A, hence the pulse power is 75 W, which currently is limited by the available driver.

Laser diodes are not limited by thermal dissipation but by so called catastrophic optical damage (COD) [5]. COD often occurs when laser diodes contain inhomogeneities that lead to non-uniform temperature profiles at the facet. Photons are absorbed near the facets and the temperature rises locally above the critical temperature destroying the laser irreversibly. This effect also occurs with short pulses. It has to be considered that laser diodes should not be operated above the maximum current rating. The outcome of this is that the laser power is limited by the applied pulse length.

Correction for color cross-talk

LEDs and laser diodes emit light in a narrow spectral region (with spectral widths of about 30 nm and 3 nm, respectively). Contrary, the red/green/blue filters of the camera sensor have much broader transmission curves which overlap with each other. As Fig. 2 shows especially, the blue and the green channel show a significant cross-talk. The transmission curves of the camera sensor filters were measured with a calibrated integrating sphere and a calibrated monochromator as adjustable light source. The monochromatic light is guided through the macro lens to the detector to determine the RGB color-value for each wavelength. The emission spectra of the LEDs were provided by the distributor. The optical throughput was calculated by pairwise integrating each emission with transmission curve over the whole spectral range from 400 m to 720 nm. The calculated values were written in a 3×3 matrix. The first row represents the throughput of the red light through the three color filters of the sensor. The second row represents the green light and the third row the blue one, respectively.

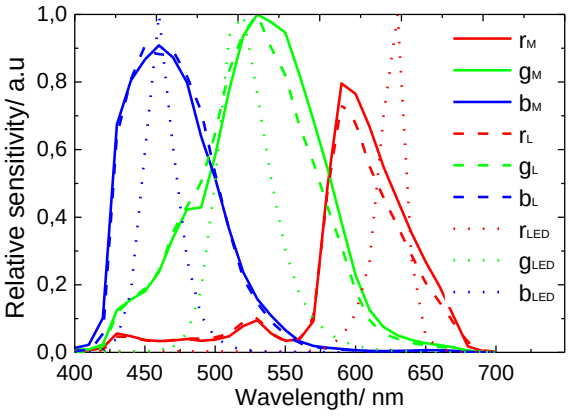

Fig. 2: Emission and transmission curves of the optical system. Solid lines: Spectral sensitivity of RGB sensor. Dashed lines: literature values for this camera [1]. Dots: spectral emission of the LEDs.

$$\begin{pmatrix} R \\ G \\ B \end{pmatrix}_{LED} = \begin{pmatrix} T_{Rr} & T_{Rg} & T_{Rb} \\ T_{Gr} & T_{Gg} & T_{Gb} \\ T_{Br} & T_{Bg} & T_{Bb} \end{pmatrix} \begin{pmatrix} r \\ g \\ b \end{pmatrix}_{image} \qquad (1)$$

The $(R,G,B)_{LED}$ values are either 1 or 0 (LED switched on or off), contrary to the T_{ij}, which are con-

tinuous and denote the integral of LED emission (i = R,G,B) multiplied with the camera filter transmission curve (j = r, g, b). The resulting matrix defines the response of the optical system to the input of the RGB LEDs. Matrix inversion then deconvolutes the measured signals to the respective input signals.

It is, however, possible to extract these parameters directly from a measured image. Due to the delay between the illumination-pulses the red, green and blue particle image is separated in space (Fig. 3, first row). In analogous manner the matrix values are inserted. T_{ij} are the color count values of the measured pixel for each color.

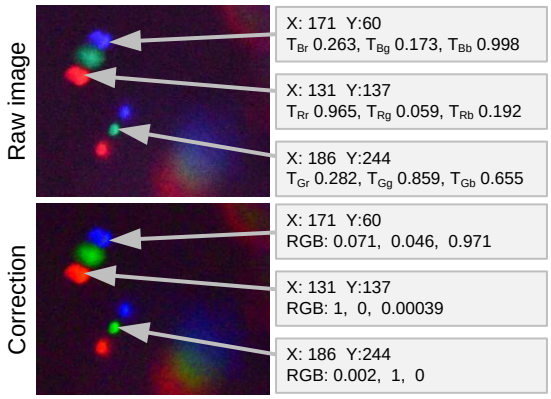

Fig. 3: first row: cross-talk of the camera filters with the emission of LEDs. Second row: corrected image using the inverted matrix.

Background correction in shadowgraph imaging

In this configuration light on its way to the detector passes 10 cm of particle seeded water. Although, most of these particles are located outside the focal plane and are not visualized on the detector, they contribute a high amount of stray light. Apparently, it is not possible to "switch of" this stray light by removing the particles because otherwise the background correction would not match to the measurement condition. Here, two approaches for a background correction are compared.

Fig. 4: Background image calculated by averaging 200 images. Traces of particles remain visible.

First, a background image was generated by averaging a large number (here 200) of images. Fig. 4 shows a close up view of a background image using this approach. It is observed that particle stray light adds noise and an intensity offset. Especially for gradient based edge detection algorithms as utilized in particle tracking techniques, such noise is an issue.

An alternative way of computing background images are the use of morphological image filters. Opening – erosion followed by dilation – is a morphological minimum filter preserving image structures larger than the structuring element. In contrast, closing – dilation followed by erosion – is a morphological maximum filter. For gray scale images erosion and dilation are respectively represented by

$$(A \ominus X)(x,y) = min\{A(x+s,y+t) - X(s,t)|(s,t)\epsilon D\} \quad (2)$$

$$(A \oplus X)(x,y) = max\{A(x+s,y+t) - X(s,t)|(s,t)\epsilon D\} \quad (3)$$

The structuring element D should closely match particle morphology and blurring due to lens aberrations. Fig. 5 shows the effect of the size of the structuring element for different particle. Here, the size of the structuring element is chosen such that the integrated intensity of particles on the background image decreases to one percent. This ensures a sufficient background correction.

For the particles used, a magnification of the optical system of 2:1 and the given detector pixel size of 7.4×7.4 µm^2 we estimated an imaged particle size of about 3 pixels for 10 µm particles and 15 pixels for 55 µm particles, respectively.

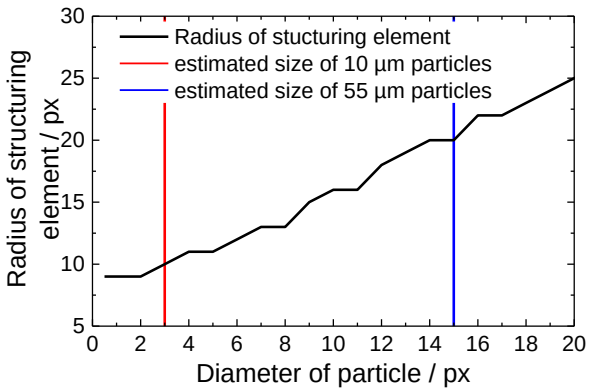

Fig. 5: The black line indicates the required radius of the structuring element so that a sufficient suppression (here 99 %) of the intensity of the particle stray-light on the background image is given. These effects were calculated for different sizes of particle images and different blurring due to the width of line spread function. The shown values represent the in-focus case with a width of the line spread function of 2.8 pixels.

For small particles blurring the edges directly increases the measured particle full width at half maximum (FWHM). Therefore, the virtual magnification of the structuring element is about a factor of two, while

the diameters of the large particles are five times bigger than the small ones.

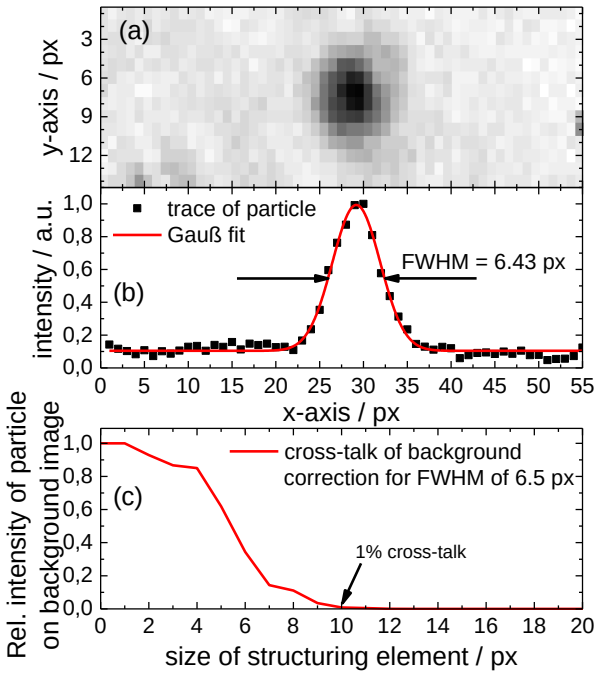

Fig. 6: Effect of morphological filtering on the background correction. In (a) a raw image of a single particle is shown. The intensity of the particle and the determination of the full width half maximum (b) is used to calculate the size of the structuring element. (c) Presents the remaining stray light of the particle in the background image depending on the size of the structuring

This method exhibits the following advantages:

- Morphological filters maximize or minimize the intensity within the radius of the structuring element. Noise or small scale variations are deleted. The computed background is smooth and unstructured.
- No distinct background images have to be taken.
- For each image an individual background correction is computed. Specific intensity variations and changes in measurement conditions are directly accounted for.

In Fig. 6, the representative FWHM of a typical particles image yields a size of about 6.5 pixels. Therefore, the structuring element should measure 10 pixels in diameter. Applying the background correction enhances the signal to noise ration from 12.5 to 20.3.

Fig. 7 presents initial results on experiments done with sprays and water suspensions and applying the described background correction procedure when LED shadowgraphic illumination, LED side-illumination or laser diodes with sheet-forming optics were employed. In the first row the colors of the shadowgraphic measurements (Fig. 7a–c) are inverted. In consequence of the subtractive color mixture red illuminated objects appear in cyan, the green ones in magenta and the blue ones in yellow. The background images for spray measurements (Fig. 7a) are acquired by averaging ten images without spray, while background images of the water tank measurements (Fig. 7b–e) are calculated by morphological filtering. To obtain the desired red/green/blue images (Fig. 7, bottom row) the background is subtracted from each raw color image

Determination of velocity fields

Particle velocity fields were calculated with the open-source toolbox PTVLab [6] for Matlab, within which a particle detection and tracking, basic background correction procedures and calibration of the length scale by processed target images are implemented.

A Gaussian-mask correlation is used to detect the position of the particles in each frame. The impact of the selected parameters, e.g. particle diameter d_p and the correlation coefficient, is calculated in [7]. With a correlation threshold value of 0.7 the Gaussian mask detects particles from 0.3 d_p up to 8 d_p having a distance from each other larger than 2 d_p. The intensity threshold should match the current particle image intensity for optimum discrimination against background noise.

The spatial displacement is calculated via cross-correlation, where the interrogation area and the cross-correlation coefficient can be adjusted. To eliminate outliers the velocity of each particle is compared to the neighbor-particle velocity assuming similar velocity vector characteristics (orientation and length). Cross-correlation generates an uncertainty in pairing particles in two time frames. Therefore, a hybrid approach [8-9] is implemented that additionally uses a relaxation method. The basic idea is that (within the given image spatial resolution) neighboring particles follow a nearly similar flow field. The environment of a particle is analyzed concerning position and distance of other particles. If, in the next time step, the neighbor particles lie within a rigidity radius, the target particle matches between two time steps.

The result of the PTVLab for several conditions is shown in Fig. 8. Images (a) and (b) show the velocity field of the water tank experiments with two sizes of seeding particles. The direction of the flow is identically, due to the same measurement position. The mean velocities differ slightly from 0.05 m/s with the 10 µm particles to 0.06 m/s with the 55 µm particles. The spray measurements (c, d) are made under similar conditions regarding fuel injection and surrounding gas stream. The differences in velocity directly came from the unsteady droplet ablation. Volume-of-fluid simulations show an oscillating ligament movement.

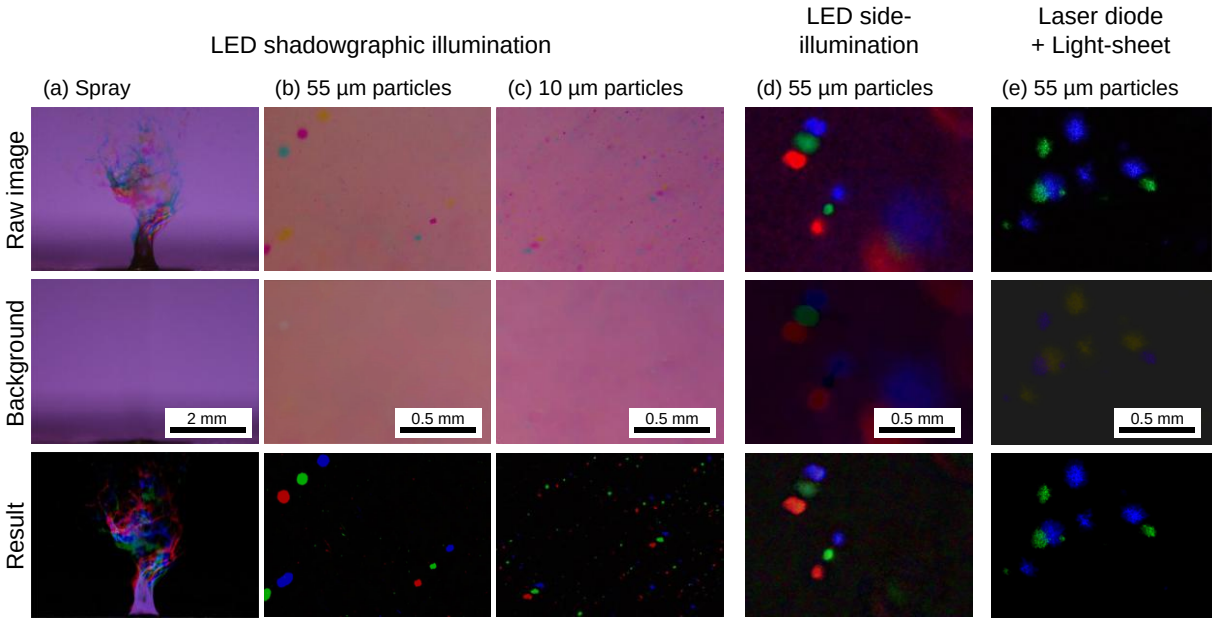

Fig. 7: Summary of raw (top row) images, background images (center row) and background subtracted images (bottom row) of the RGB images as input for PTVLab. Each column is an example for one of the three illumination techniques (shadowgraphy, side illumination, laser light sheet) utilized in the present experiments. For a better assessment of the captured images and background correction image sections are shown.

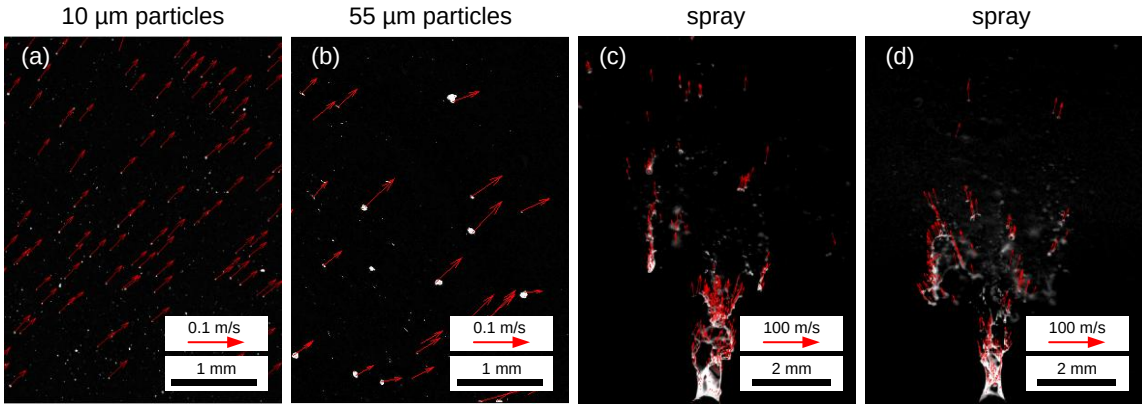

Fig. 8: Velocity fields for 10 µm (a) and 55 µm (b) particles. The images were taken at the same location in the water tank, therefore nearly similar velocity vectors were determined. Two sprays at different moments are shown in (c,d). The unsteady droplet ablation and the liquid ligaments directly above the nozzle can be seen.

Conclusions

We demonstrated the application of low-cost color light sources and detectors with RGB Bayer filter and for particle tracking velocimetry. Three different combinations of geometric arrangement and light sources were compared: Shadowgraphy (back illumination) with high-power LEDs, flood illumination from the side with the same LEDs, and sheet illumination from the side using laser diodes.

The shadowgraph arrangement provides better discrimination of the particles against the background than the side-illumination arrangement. This results in a higher number of detected particles, better particle tracking capabilities and a simpler background correction algorithm. One disadvantage of the 90° alignment is the difficulty in eliminating out-of-focus particles. Point light sources outside the depth of field generate the so called circle of confusion [10]. The edges of the out-of-focus objects feature a steep gradient and thus are not distinguishable from in-focus objects. In shadowgraphic illumination the light source is much bigger. The out-of-focus objects are blurred and can be eliminated with relatively simple algorithms. Using laser diodes with sheet-forming optics can drastically

reduce the problems associated with out-of-focus particles, but laser diodes are much more sensitive against excessive forward current than LEDs, thus overdriving them in pulsed operation is not possible.

While these three experiments were performed in a particle-seeded container filled with water, we also show some results from RGB-visualization of a spray (from our previous work reported in [4]). Here, shadowgraphy was applied and it works very well for qualitative assessment of the complex structure of this particular spray. However, because of this structure, reliably deriving velocities via PTV is not possible everywhere in the spray, but only where suitable structures exist.

Acknowledgements

The authors acknowledge technical support by A. Krasowsky. This work was funded by the German Research Foundation (DFG) within SCHU 1369/14.

References

[1] J. Jiang, D. Liu, J. Gu, S. Susstrunk, Appl. Comput. Vision (2013) 168-179.
[2] J. Estevadeordal, L. Goss, in 43rd AIAA meet (2005) 12355-12364.
[3] M. Sommerfeld, D. Bröder, Ind. Eng. Chem. Res. 48 (2009) 330-340.
[4] C. Weise, J. Menser, S. A. Kaiser, A. Kempf, I. Wlokas, Proc. Combust. Inst. 35 (2015) 2259-2266.
[5] M. Bou Sanayeh, Appl. Phys. Lett. 89, 101111 (2006).
[6] W. Brevis, Y. Niño, G. Jirka, Exp Fluids 50 (2011) 135-147.
[7] K. Takehara, T. Etoh, J Vis 1 (1999) 313-323.
[8] W. Brevis, Y. Niño, G. H. Jirka, Exp Fluids 50 (2011) 135-147.
[9] P. Jia, Y. Wang, Y. Zhang, Meas. Sci. Technol. 24 (2013) 055301.
[10] A. Levin, R. Fergus, d. Durand, W. T. Freeman, ACM Trans. Graph. 26 (2007) 70.